ELSEVIER

Journal of Nuclear Materials 244 (1997) 51–58

journal of nuclear materials

TEM and IBA study of the thermal oxidation of V following high dose He implantation

P.W. Gilberd [a,*], P.B. Johnson [a], I.C. Vickridge [b], A.C. Wismayer [c]

[a] *Department of Physics, Victoria University of Wellington, PO Box 600, Wellington, New Zealand*
[b] *The Institute of Geological and Nuclear Sciences Ltd, PO Box 31312, Lower Hutt, New Zealand*
[c] *The Open Polytechnic of New Zealand, PO Box 31914, Lower Hutt, New Zealand*

Received 3 June 1996; accepted 22 November 1996

Abstract

High dose He implantation in V can lead to the formation of He bubble arrays with high cavity volume fractions. These structures, which are of interest in relation to applications such as catalysis, are characterized by nanoscale cavities of uniform size separated by microscopically thin metal walls. The oxidation of such structures with volume fractions of approximately 20%, is investigated. High levels of lateral stress are evident in the implanted V specimens. A combination of TEM and IBA is used to show that when such structures are thermally oxidized in flowing oxygen at temperatures up to 400°C: (i) an abrupt interface is maintained between the growing oxide layer and the underlying V (which is also the case for compact V); (ii) the underlying bubble structure is preserved; (iii) unexpectedly, the oxygen uptake is slightly inhibited compared with that for compact V, and; (iv) the formation of V_2O_5 is favored over V_3O_7 when compared with compact V.

1. Introduction

Helium is insoluble in metals and precipitates out to form gas bubbles. For high dose helium implantation at temperatures $\simeq 0.2\ T_m$ (where T_m is the melting temperature of the metal) the bubbles are in high concentration $\simeq 2 \times 10^{25}\ m^{-3}$ (see for example, Refs. [1–10]). As the bubble array coarsens with increasing dose, the bubble concentration falls but the cavity volume fraction ($\Delta V_b/V$) increases [7–10]. These coarser bubble arrays are characterized by a high degree of cavitation (i.e., a high cavity volume fraction). Very little is known of the chemical and physical properties of such implanted surfaces. A high degree of cavitation might be expected to increase the chemical activity, whereas the high levels of biaxial compressive stress in planes parallel with the surface — the lateral stress — might be expected to lower the activity by restricting atomic transport through the surface.

The present work was prompted in part by the possibility that heavily cavitated layers prepared in metal surfaces by helium ion implantation could have unique chemical properties. Here we examine the oxidation of such surfaces in vanadium. Vanadium was chosen for this first TEM/ion beam analysis (IBA) study for a variety of reasons including: (i) of all the metals, it has one of the most complex oxide systems and so provides a potentially rich area of research into the chemical activity of helium implanted surfaces; (ii) it was the metal used in the most detailed previous studies of the cavity structures formed by helium implantation [6–8,10]; (iii) it was the metal used in a recent investigation into the use of Raman spectroscopy for the study of oxidation in thin implanted layers [11]; and (iv) the vanadium oxides have particular potential in catalytic applications and as lithium intercalators in lithium battery technology.

In considering the microstructural changes in metals resulting from gas implantations, a further source of interest arises from the possible influence such changes may have on the operation of controlled thermonuclear fusion reactors (see for example, Refs. [12–18]). Vanadium and vanadium-based alloys are potential candidate metals for fusion systems [14–17]. The primary containment wall and other plasma-facing surfaces, such as metals used for

* Corresponding author. Fax: +64-4 495 5237.

PII S0022-3115(96)00726-X

selective helium pumping at the plasma boundary [14,17], will be bombarded by helium produced in nuclear reactions in the plasma. Helium induced cavity structures in plasma-facing metals have been investigated, for example, by Bein et al. [17] and by Muroga et al. [18]. In a given device, the precise nature of the cavity structure will depend, of course, on many factors including the implantation history, operating surface temperature and exposure to thermal transients involving high heat loadings [16,18]. Knowledge of the physical and chemical properties of highly cavitated vanadium surfaces is of interest in this context, also.

For monoenergetic helium implantation in copper, a proposed model for the development of the bubble structure with depth below the surface and with increasing helium dose has been reported elsewhere [9]. In the case of vanadium, the evidence is consistent with the model proposed for copper [10]. The results for both metals are consistent with the proposition that the bubble growth, at least in the later stages of bubble development, is driven mainly by the local helium concentration in the matrix rather than by the damage.

A striking feature of the bubble structures at matrix helium levels around 10 at.% is the ordering of gas bubbles to form a gas-bubble superlattice [1–10] consisting of small helium bubbles of very uniform size ($\simeq 2$ nm diameter) at high concentration (nearest neighbor distance $\simeq 4$ nm). With increased helium dose, the bubble array remains ordered as it coarsens [8–10]. At high dose levels, corresponding to helium concentrations beyond 20 at.%, the bubble arrays are less well ordered. The ordered stages at low and medium helium dose levels are thought to be centrally important in seeding the unique characteristics of the random cavity structures found at the higher helium concentrations. Structures beyond the superlattice stage are characterized by nanoscale cavities of uniform size and metal 'walls' separating nearest-neighbor cavities which are thin on a microscopic scale [7,10]. In the present work we use TEM and IBA techniques to investigate the oxidation of vanadium surfaces containing cavity structures which retain some degree of cavity ordering, but are on a coarser scale than the superlattice stage of bubble development.

2. Experimental procedure

Vanadium foil, 99.8% pure, 25 μm thick, from Goodfellow Metals was diamond polished in stages down to 1 μm diamond paste and annealed at 1200°C for 2 h in vacuum. The samples were implanted with 160 keV helium at 60° to the surface normal. For these conditions, the distribution of implanted helium with depth below the target surface calculated using TRIM-95 [19] is a bell-shaped curve centered on a depth of approximately 300 nm. The results are broadly similar to those already published for copper [9] and so are not presented here. Ion doses ranged from the critical dose for blistering, Φ_c ($\simeq 10^{22}$ He^+ ions m^{-2} in our conditions), down to $0.55\Phi_c$. The incident beam was scanned over an area of approximately 1.5 cm^2 during the implantation. The beam dose uniformity, judged by the visible onset of blistering and observation by TEM of the uniformity of bubble structures, is estimated to be within $\pm 10\%$ over a 1 cm^2 central region. The sample temperature was maintained near 160°C (0.2 T_m, where T_m is the melting point of vanadium) during the implantation.

Following ion implantation, up to nine 3 mm discs were punched from the implanted region. Where necessary, the surface layers were removed to expose bubble structures with high cavity volume fractions. Such erosion was effected with a 30 μA, 4 keV argon beam directed onto the front (implanted) surface of the sample, at 30° to the surface normal, while the sample was rotated. Ion milling times ranged from 10 min to 4 h. The samples were held under a tantalum mask; tantalum being conventionally favored because of its low sputtering coefficient.

Oxidations were performed using a conventional flow furnace of volume 150 ml in a 99% oxygen 1% argon atmosphere with gas flow rate of 20 ml min^{-1}. Temperatures below 0.5 T_m [20] were chosen in an attempt to preserve the underlying cavitation through the oxidation process.

2.1. Sample analysis

Samples were back-thinned for TEM either by wet chemical jet thinning to perforation (typically taking about 1 min) with a 15% H_2SO_4 in CH_3OH solution (with the implanted/oxidized face protected by Mylar film), or by ion beam milling to perforation (which typically took some tens of h). TEM was performed with a Philips 420 microscope, at an accelerating voltage of 100 keV.

Ion Beam Analysis was carried out in a general purpose IBA chamber on a vertical KN3000 Van de Graaff accelerator, described in Ref. [21]. For Rutherford backscattering spectrometry (RBS), a 2 MeV α-particle beam was used, with particle detection at 165°. Areal densities of oxygen were determined by nuclear reaction analysis (NRA) via the $^{16}O(d, p_1)$ reaction. The protons generated by the 950 keV incident deuteron beam were detected in a 300 mm^2 silicon surface barrier detector at 150°. A 13 μm Mylar film prevented elastically-scattered deuterons from swamping the detector.

3. Results and analysis

3.1. Annealed vanadium

Electron diffraction indicates that annealing resulted in most of the vanadium crystals having the [111] direction

normal to the surface. NRA showed a bulk global composition of approximately 4 at.% of oxygen after annealing. This is above the solubility limit for oxygen [22]. Thin platelets of the α′ oxide phase containing up to 12 or 13 at.% of oxygen [23] were found in a matrix of α-phase vanadium which contained oxygen in dilute (less than 4 at.%) solid solution. Extensive regions free of α′ oxide phase were observed and all TEM results pertain to such regions.

3.2. Implanted vanadium

Representative bubble structures having high cavity volume fractions are shown in Fig. 1. The bubble structure of a sample irradiated to a dose of $0.7\Phi_c$ is shown in Fig. 1a. The bubbles vary in diameter from 2.0 to 3.5 nm. The estimated cavity volume fraction is 20%. This stage of bubble development is beyond the superlattice stage (which extends to cavity volume fractions of up to 10%).

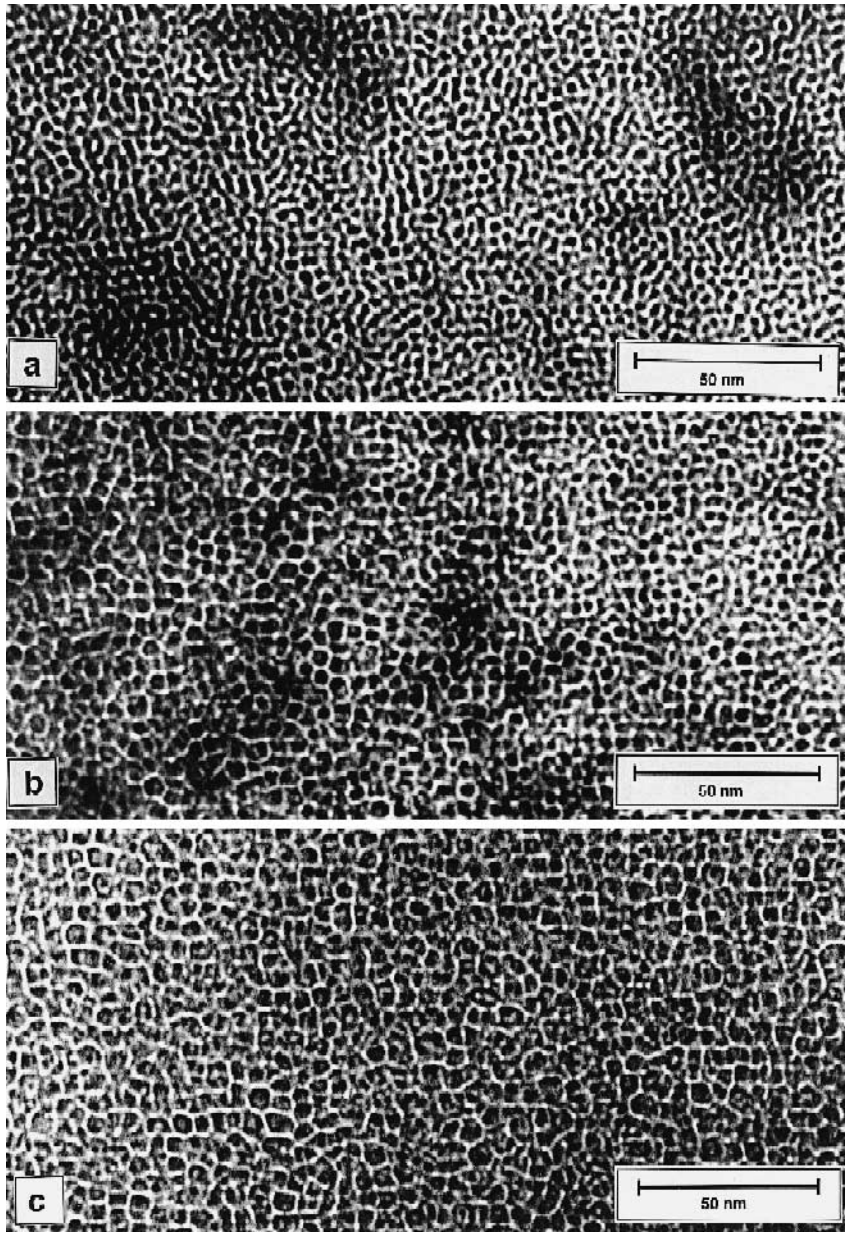

Fig. 1. (a) Bubble structure of a sample irradiated to $0.7\Phi_c$ and prepared for TEM by jet-thinning. (b) Bubble structure of a sample irradiated to $0.95\Phi_c$ (prepared by jet-thinning). (c) Bubble structure of a sample irradiated to $0.95\Phi_c$ (prepared by ion beam thinning).

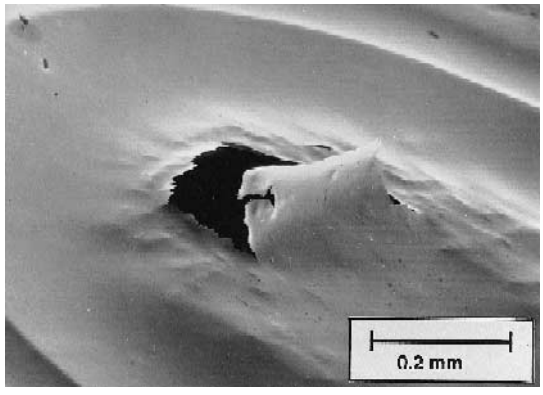

Fig. 2. An implanted vanadium sample, jet-thinned to perforation, showing catastrophic rupture. The jet was directed onto the back of the sample (i.e., directed into the page). The deformation in the thicker regions of the specimen is *into* the jet (i.e., away from the front surface) whereas the deformation in the thinner regions of the specimen is *away* from the jet.

Coarser bubble structures in samples irradiated to a dose of $0.95\Phi_c$ are shown in Fig. 1b, c. The specimen of Fig. 1b has been jet-thinned from the back. The bubbles vary in diameter from 2.5 to 5.0 nm. The specimen of Fig. 1c has been thinned from the back using ion-beam erosion. In this case the bubbles vary in diameter from 3.0 to 7.0 nm. The structure in Fig. 1a, which could be prepared more reproducibley than the more advanced cavity structures, was selected for the first TEM/IBA studies of oxide formation described below. In terms of stages of bubble development, this structure is bounded on the low dose side by the gas-bubble superlattice stage and on the high dose side by the structure of Fig. 1b, c.

When using jet back-thinning it has been found that perforation is invariably accompanied by substantial distortion of the region surrounding the hole (Fig. 2). It is known that the deposition of gas and damage during ion-implantation can result in a strong biaxial compression — the lateral stress — developing in planes parallel with the target surface. The nature of the distortion in Fig. 2 provides dramatic evidence of the high levels of lateral stress in the targets investigated here. Notice that in the thinnest regions of the target around the hole, the curvature is towards the front (implanted) surface, whereas in the thicker regions, away from the hole edge, the curvature is towards the back surface (i.e., against the electrolyte flow direction). This pattern of strain is consistent with the lateral stress reaching a maximum at a depth below the surface (presumably corresponding to a depth near the maximum in the implanted helium concentration) rather than at the surface itself.

It has been found that back-thinning using ion beam erosion, although much slower, circumvents the catastrophic rupture evident in Fig. 2, possibly by relieving the lateral stress in the ion implanted vanadium more gradually. Ion beam thinning has two further advantages. It preserves the bubble structure better than electrochemical thinning and is less likely to destroy any surface oxides in oxidized samples.

RBS showed contamination in the samples after implanting and ion beam thinning. This is almost certainly tantalum from the mask in the ion beam thinner. Tantalum is a simple group V substitutional impurity in vanadium and at the low contamination levels found here (less than 1 at.%) is expected to have no significant effect on the system.

3.3. Oxide thickness

3.3.1. Compact vanadium

In Fig. 3 we present the oxide thickness, determined by NRA, for compact vanadium which had been prepared in the same way as the implanted samples, except that no implantation nor ion beam thinning was performed. At 450°C the oxide thickness is proportional to $t^{1/2}$, where t is the time of oxidation, indicating that the oxidation rate is limited by the diffusion of reaction products through the growing oxide layer. At the lower temperatures the oxide thickness follows a $\log(t)$ law, indicating a more complex oxidation process, possibly with a time-variable diffusion cross-section for the mobile species traversing the growing oxide layer [24]. We also performed RBS on these samples, and a representative selection of results is shown in Fig. 4. Below 450°C the oxide has a relatively abrupt interface with the underlying vanadium. This indicates that there is very little diffusion of oxygen from the growing oxide layer into the bulk of the vanadium. By 450°C, slight interface broadening is evident and a small amount of oxygen penetrates deeper into the vanadium. This deeper oxygen is also evident in NRA spectra. It should be noted that the slope of the RBS edge provides only an upper limit for the width of the interface between the vanadium

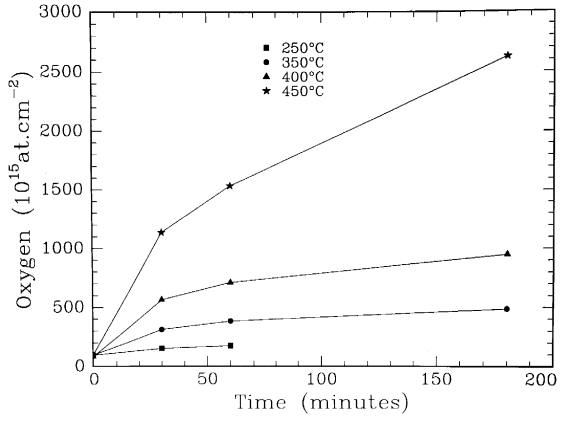

Fig. 3. Oxygen uptake by compact vanadium as a function of time after thermal oxidation in flowing O_2, at four temperatures covering the range from 250–450°C.

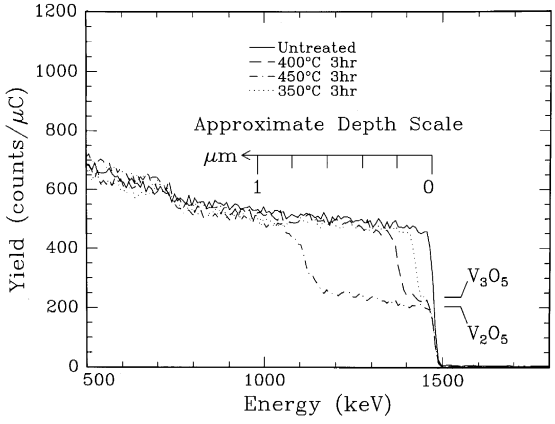

Fig. 4. RBS spectra from compact vanadium oxidized for 3 h at different temperatures. Also shown for comparison is the RBS spectrum of an unoxidized compact vanadium sample. The indicative depth scale has been calculated for a composition of V_2O_5, but is accurate to within about 10% for the other oxide phases. The theoretical plateau heights for two oxide phases, which span the range of oxides observed in the present work, are also shown.

and the vanadium oxide, since surface roughness (which cannot be excluded here) would have an identical effect in broadening the RBS spectrum. The overall conclusion is that, up to 450°C, there is very little penetration of oxygen into the bulk vanadium.

3.3.2. Implanted vanadium

The studies of the oxidation of implanted surfaces centered on specimens having a cavity structure, similar to that shown in Fig. 1a, exposed at the surface, where necessary, by ion beam milling. There was some variability possible in the structure at the surface in the different specimens because of the uncertainties associated with the helium implantations and the amount of material removed by ion beam milling. However, the results of NRA and RBS analyses of the oxidized surface allow us to make some qualitative observations. Firstly, the implanted substrate does not increase the oxidation rate at all — in fact it has a slight inhibitory effect, a point we take up later. Secondly, even though the layer containing bubbles is several hundreds of nm in thickness, RBS results show no difference in the broadening of the oxide–vanadium interface between implanted and compact vanadium. The results indicate that there is little if any interconnection of the cavities near the front surface of the specimens studied — at least in so far as oxygen transport is concerned.

3.4. Oxide structures

Since the unit cells for oxides of vanadium tend to be large (often $\simeq 1$ nm), crystallites of vanadium oxide can be distinguished from the vanadium matrix by the appearance of lattice fringes. For the Philips TEM used in this

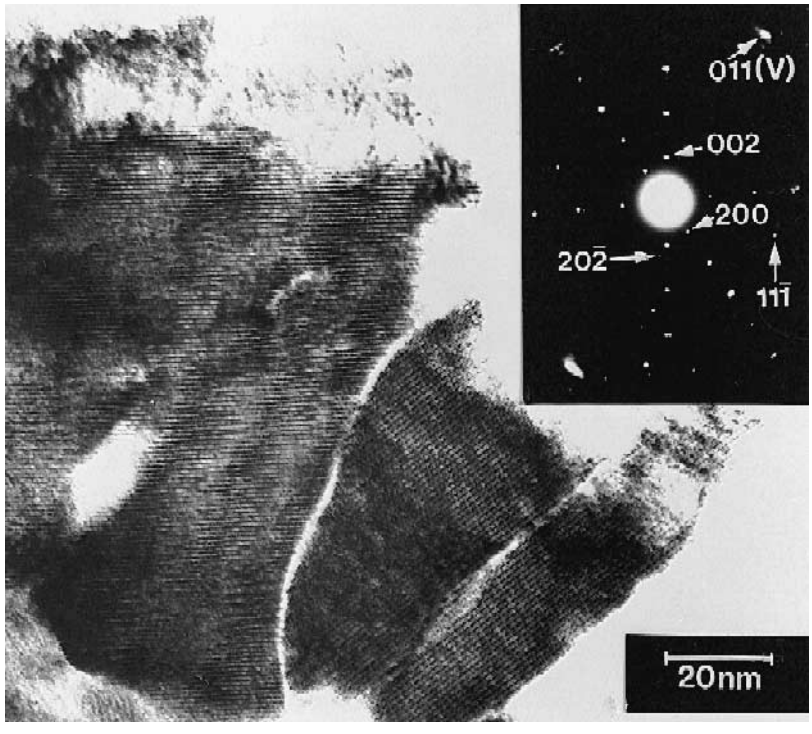

Fig. 5. Lattice fringe images of an oxide phase on an implanted sample which has been oxidized at 350°C for 30 min, following removal of the front surface by ion beam thinning. The inset diffraction pattern is from a somewhat larger area than that shown in the micrograph.

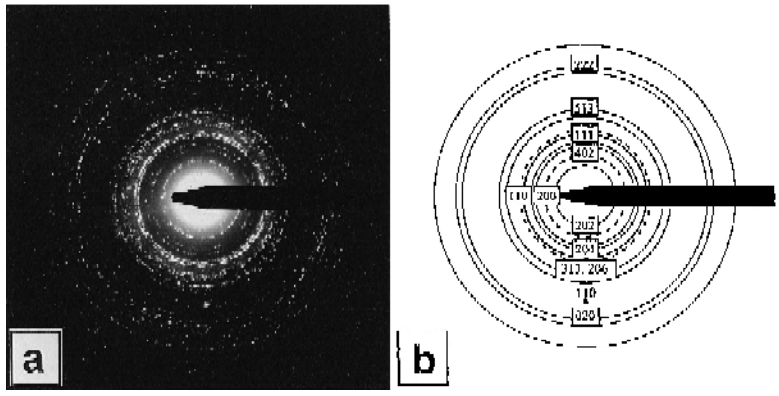

Fig. 6. (a) Ring electron diffraction pattern typical of those observed from compact vanadium oxidized at 400°C. The vanadium 110 spot is also visible. (b) Schematic diagram of the electron diffraction pattern showing the main rings only: ———— V_3O_7; --- V_2O_5.

work, fringes of 0.5 nm are readily observable and it is seen that, for both compact and implanted vanadium, the oxides appear as thin rectangular plates, a few nm thick, and typically 100 nm long by 30 nm across. Invariably, the lattice fringes run parallel to the long axis of the crystallite. Overlapping crystallites are often observed.

Fig. 5 shows lattice fringe images of an oxide phase on a sample implanted to $0.7\Phi_c$. The front surface was removed by ion beam thinning prior to jet-thinning to perforation from the back. The sample was oxidized at 350°C for 30 min before TEM examination. Two large crystallites are evident. The ratio of the two largest fringe spacings, measured from the bright-field image, and also from the diffraction pattern (inset), is 1.19. These fringes can be ascribed to the (200) and (002) planes of V_3O_7. The diffraction pattern also shows reflections from other planes, including $(11\bar{1})$ and $(20\bar{2})$, for which the contributing crystallites lie outside the area covered by the micrograph. These reflections confirm that the observed oxide phase is V_3O_7. The bubble structure is no longer evident, being masked by the oxide, but reappears in the image when the oxide is removed from the surface by ion beam thinning for a few min. We have also confirmed that the bubble structure is preserved after oxidation at 400°C (0.34 T_m). The phase V_3O_7 has been observed both in compact and implanted vanadium, and at oxidation temperatures of 350°C and 400°C. At 350°C, VO_2 is also produced.

At 400°C, V_3O_7 is the dominant phase in compact vanadium. Fig. 6a shows the electron diffraction pattern for a sample of annealed vanadium which has been oxidized at 400°C for 1 h and then subsequently thinned from the back with an argon ion beam. Fig. 6b shows that most of the pattern is due to V_3O_7 but that two rings are consistent with a second phase, ascribed to V_2O_5. A similar result is obtained with just 15 min oxidation. An implanted sample which had not been ion beam thinned from the front was oxidized for 15 min and then prepared for TEM by jet-thinning. The diffraction pattern (Fig. 7a) is consistent with that for V_2O_5 alone (Fig. 7b), although persistence of V_3O_7 has been observed in other samples of highly cavitated vanadium oxidized under identical conditions. These results suggest that in highly cavitated vana-

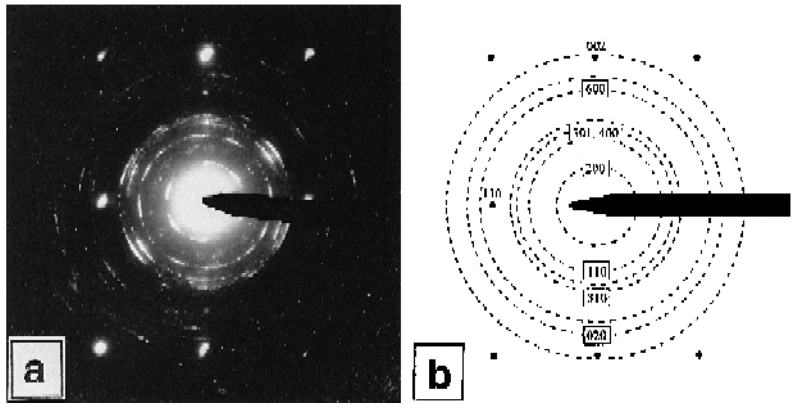

Fig. 7. (a) Ring electron diffraction pattern typical of those observed from implanted vanadium oxidized at 400°C. The vanadium 110 and 002 spots are also visible. (b) Schematic diagram of the electron diffraction pattern showing main rings only: --- V_2O_5.

dium the formation of V_2O_5 is enhanced over V_3O_7. Oxidation of implanted surfaces at 350°C has also been observed to promote the formation of V_2O_5 at the expense of V_3O_7.

Often, diffraction patterns from oxidized samples show that the {101} atomic planes give rise to split spots, with the splitting consistent with the body centered tetragonal β phase ($a = 0.299$ nm, $c = 0.326$ nm), rather than the body-centered-cubic α phase ($a = 0.304$ nm). The onset of the tetragonal phase is $VO_{0.18}$, indicating that at least some of the vanadium matrix has been oxidized to this level.

4. Discussion

For the conditions used for the argon ion-beam erosion of specimens, calculations performed with TRIM-95 [19] for compact vanadium indicate that the mean depth of the damage distribution due to the argon ion-beam is less than 5 nm. Further, most of the damage is confined to depths less than 10 nm. These distances are much less than the thickness of the TEM specimens and we conclude that damage structures from the ion beam thinning are not a major feature of the micrographs.

For both compact and implanted vanadium substrates the oxidation kinetics and preferred phases depend very sensitively on temperature between 350°C and 450°C. The highly cavitated vanadium on which oxides have been grown has influenced the thermal oxidation process; compared with compact vanadium, a different phase composition is obtained. Furthermore, an inhibition of thermal oxidation is found. It is known that the ion implantation of suitable atomic species can improve the corrosion resistance of metals. However, to our knowledge such an effect has not previously been reported for high dose inert gas implantations. In fact Rao et al. [25] have found the reverse effect. For nickel, they found that the physical effect of inert species implantation (krypton and nickel) was to increase the oxidation rate of the implanted surface. This was attributed to increased nucleation sites for NiO formation.

One could speculate that the inhibition of oxidation in the present case results at least in part from a reduction in mobility of vanadium interstitials and/or oxygen atoms in the vanadium matrix owing to high levels of lateral stress in the implanted surface. This is somewhat surprising given the high degree of cavitation involved. It could be expected that this inhibition will be more than offset if a fully developed nanoporous layer (such as the cavity structure shown in Fig. 1c) were to be exposed at the specimen surface. Certainly, for a blistered surface we have found oxide formation to be considerably enhanced.

It is satisfying that the plateau heights observed in the RBS spectra, which indicate the overall oxygen content of the oxide films, are consistent with the phase compositions observed by TEM. However, it must be pointed out that the plateau heights are not a particularly sensitive indicator of overall oxygen content. This may be judged from the theoretical plateau heights shown in Fig. 4. Furthermore, the NRA method for oxygen determination does not have the depth resolution to allow authoritative statements about the overall stoichiometry of the thin oxide films.

The pore sizes in the substrates used in the present study (Fig. 1a) were larger than those typical of a fully ordered bubble superlattice but less than those of the highly swollen structure associated with higher doses (Fig. 1b, c). To prepare as large an area as possible on a given vanadium sheet for these oxidation studies, the helium beam was scanned over a larger area than has been previously used. As a result the beam current density is lower here than in earlier studies. The bubble sizes are smaller than we would expect for the total helium doses used, which may indicate a dose-rate dependence for the formation of the helium bubble structures in vanadium. In this context it is interesting to note that dose-rate dependencies for the onset of blister formation have been found in other gas/metal systems [26–28].

Overall, these first results show an influence of the implanted (high cavity volume fraction) vanadium substrate on the rate of oxide formation and on the phase of the oxide. Other workers have shown that the nature of the substrate influences the catalytic properties of V_2O_5 [29]. This suggests that it would be interesting to determine the oxidation kinetics and the chemical properties of vanadium oxides for substrates with even higher cavity volume fractions.

5. Conclusion

TEM and IBA have been successfully used to identify and characterize thin oxide layers on compact and implanted vanadium. In particular, we have shown that:

(1) There is a high level of lateral stress present in helium implanted layers.

(2) Unexpectedly, the oxidation of vanadium containing bubble structures with a high cavity volume fraction of approximately 20%, is still slightly inhibited compared with the oxidation of compact vanadium. This is attributed to an effect of lateral stress.

(3) There is a sharp boundary between the high oxygen stoichiometry thermal oxide and the underlying α/β phase vanadium in both implanted and compact vanadium at temperatures up to at least 450°C.

(4) The bubble structures formed by high dose helium implantation into vanadium are preserved during thermal oxidation at temperatures up to at least 400°C.

(5) The thermal oxide formed at 400°C on an implanted substrate contains an appreciable amount of V_2O_5, whereas the 400°C thermal oxide formed on a compact vanadium substrate contains predominantly V_3O_7. This may reflect a

general tendency to form higher stoichiometry oxides on helium-implanted surfaces.

Acknowledgements

This work was performed under a research contract to the New Zealand Foundation for Research, Science and Technology. It gives us great pleasure to acknowledge the assistance given to this work by the contributions of T. Lundy, R. Thomson, Y. Morrison and T. Young of Victoria University of Wellington, and of W. Trompetter and C. Purcell from Geological and Nuclear Sciences. The authors also thank E. Maydell and D. Fabian for their critical reading of the draft manuscript.

References

[1] D.J. Mazey, B.L. Eyre, J.H. Evans, S.K. Erents and G.M. McCracken, J. Nucl. Mater. 64 (1977) 145.
[2] P.B. Johnson and D.J. Mazey, Nature 276 (1978) 595.
[3] P.B. Johnson, A.L. Malcolm and D.J. Mazey, Nature 329 (1987) 316.
[4] P.B. Johnson, A.L. Diprose and D.J. Mazey, J. Nucl. Mater. 158 (1988) 108.
[5] P.B. Johnson, R.W. Thomson and D.J. Mazey, Nature 347 (1990) 265.
[6] P.B. Johnson, K.J. Stevens and R.W. Thomson, Nucl. Instrum. Meth. B62 (1991) 218.
[7] P.B. Johnson, in: Fundamental Aspects of Inert Gases in Solids, eds. J.H. Evans and S.E. Donnelly (Plenum, New York, 1991) p. 167.
[8] P.B. Johnson and D.J. Mazey, J. Nucl. Mater. 218 (1995) 273.
[9] P.B. Johnson, K.L. Reader and R.W. Thomson, J. Nucl. Mater. 231 (1996) 92.
[10] P.B. Johnson and P.W. Gilberd, in: Proc. of the 10th Int. Ion Beam Modifications of Materials Conf. (IBMM-96), Albuquerque, NM (1996), Nucl. Instrum. Meth., in press.
[11] P.W. Gilberd, P.B. Johnson and I.C. Vickridge, in: Proc. of the 10th Int. Ion Beam Modifications of Materials Conf. (IBMM-96), Albuquerque, NM (1996), Nucl. Instrum. Meth., in press.
[12] P.B. Johnson and T.R. Armstrong, Nucl. Instrum. Meth. 148 (1978) 85.
[13] S.E. Donnelly, Radiat. Eff. 90 (1985) 1.
[14] J.N. Brooks and R.F. Mattas, J. Nucl. Mater. 121 (1984) 392.
[15] B.A. Loomis and D.L. Smith, J. Nucl. Mater. 191–194 (1992) 84.
[16] J.N. Brooks, D.N. Ruzic, D.B. Hayden and R.B. Turkot, Jr., J. Nucl. Mater. 220–222 (1995) 269.
[17] B.K. Bein, J. Bolte, G. Kalus, D. Kurowski, J. Gibkes, K. Brand, M. Chirtoc and J. Pelzl, J. Nucl. Mater. 220–222 (1995) 805.
[18] T. Muroga, K. Dohi, Y. Ishihama, K. Tokunaga and N. Yoshida, J. Nucl. Mater. 191–194 (1992) 1248.
[19] J.F. Ziegler, J.P. Biersack and U. Littmark, The Stopping and Range of Ions in Matter (Pergamon, New York, 1985).
[20] P.B. Johnson, D.J. Mazey and J.H. Evans, Radiat. Eff. (1983) 147.
[21] I. Vickridge, J. Tallon and M. Presland, Nucl. Instrum. Meth. B85 (1994) 95.
[22] W. Rostoker and A.S. Yamamoto, Trans. Am. Soc. Metals 47 (1955) 1002.
[23] K. Hiraga, H. Ikeda and M. Hirabayashi, Jpn. J. Appl. Phys. 19 (1980) 397.
[24] D.E. Davies, U.R. Evans and J.N. Agar, Proc. R. Soc. A225 (1954) 29.
[25] Z. Rao, J.S. Williams and D.K. Sood, Nucl. Instrum. Meth. B106 (1995) 538.
[26] H. Verbeek and W. Eckstein, in: Application of Ion Beams to Metals, eds. S.T. Picraux, E.P. Ernisse and F.L. Vook (Plenum, New York, 1974) p. 597.
[27] W. Möller, Th. Pfeiffer and D. Kamke, in: Ion Beam Surface Layer Analysis, eds. O. Meyer, G. Linker and F. Käppler, Vol. 2 (Plenum, New York, 1976) p. 842.
[28] T.R. Armstrong, PhD thesis, Victoria University of Wellington, New Zealand (1980).
[29] H. Bosch and F. Janssen, Catal. Today 2 (1988) 369.